Growth of epitaxial AlN(0001) on Si(111) by reactive magnetron sputter deposition

I. Ivanov, L. Hultman, K. Järrendahl, P. Mårtensson, J.-E. Sundgren, B. Hjörvarsson, and J. E. Greene

Citation: Journal of Applied Physics **78**, 5721 (1995); doi: 10.1063/1.359632
View online: http://dx.doi.org/10.1063/1.359632
View Table of Contents: http://scitation.aip.org/content/aip/journal/jap/78/9?ver=pdfcov
Published by the AIP Publishing

Growth of epitaxial AlN(0001) on Si(111) by reactive magnetron sputter deposition

I. Ivanov, L. Hultman, K. Järrendahl, P. Mårtensson, and J.-E. Sundgren
Department of Physics, Linköping University, S-581 83 Linköping, Sweden

B. Hjörvarsson
Department of Physics, Uppsala University, Box 530, S-751 21 Uppsala, Sweden

J. E. Greene
Department of Materials Science, the Coordinated Science Laboratory, and the Materials Research Laboratory, University of Illinois, Illinois 61801

(Received 27 April 1995; accepted for publication 29 June 1995)

2H–AlN(0001) layers have been grown on Si(111) by reactive magnetron sputtering from an Al target in $Ar+N_2$ gas mixtures at temperatures $T_s=400$–900 °C. Variations in reactive gas consumption, target voltage, and current–voltage characteristics versus nitrogen partial pressure were used to determine deposition parameters required to yield stoichiometric AlN with growth rates ≥ 2 μm h^{-1}. High-resolution cross-sectional transmission electron microscopy (XTEM) analyses of films grown at 900 °C showed that the initial 6–8 monolayers were (111)-oriented cubic 3C before transforming to the (0001)-oriented 2H polytype. The epitaxial relationship was found by XTEM and x-ray diffraction (XRD) to be 2H–AlN(0001)//3C–AlN(111)//Si(111) with 2H–AlN[$1\bar{2}10$]//3C–AlN[110]//Si[110]. High-resolution XRD $\omega-2\Theta$ and ω rocking curve widths for films grown at $T_s=900$ °C were 70 and 500 arc sec, respectively, the lowest values yet reported. © *1995 American Institute of Physics.*

I. INTRODUCTION

The wide-band-gap group III nitrides, AlN, GaN, and InN, are of interest for high-temperature and optoelectronic device applications. AlN is an insulator with a direct band gap (6.2 eV), a large thermal conductivity (260 W m^{-1} K^{-1}), and high thermal and chemical stability. The equilibrium form of AlN at room temperature is the wurtzite structure, but metastable zinc-blende and NaCl structure AlN have also been reported.[1] A variety of techniques including chemical-vapor deposition (CVD),[2,3] reactive molecular-beam epitaxy (MBE),[4] and sputtering[5–10] have been used to grow AlN. The CVD process typically requires growth temperatures in excess of 900 °C for the dissociative adsorption of N from either NH_3 or N_2. AlN films with the best crystalline quality, as judged by x-ray diffraction (XRD), have been obtained by metal-organic CVD (MOCVD) on $Al_2O_3(0001)$ at $T_s=1000$ °C. XRD $\omega-2\Theta$ rocking curves from ~1-μm-thick layers were reported to have a full width at half-maximum (FWHM) intensity of 97.2 arc sec.[11]

Most AlN films deposited by sputter deposition have been polycrystalline,[6–9] although epitaxial layers have been obtained on a variety of substrates.[10] Several reports have shown that the N_2 partial pressure during sputter deposition plays a crucial role in determining nitride film stoichiometry and crystallinity.[12–15] Lewis, Glocker, and Jorne[16] measured the secondary electron emission coefficient γ for Al (and Ti) bombarded with Ar^+, N_2^+, and $Ar^+ + N_2^+$ ions with energies between 350 and 700 eV. Variations in γ with adsorbed N coverage were then used in analyzing the reactive sputtering process.

In this article we report results on the use of reactive magnetron sputter deposition to grow epitaxial AlN on Si(111) substrates. Nitrogen gas consumption, target voltage, and current–voltage characteristics versus N_2 partial pressure were used as diagnostic probes to optimize the deposition process. Film stoichiometry was determined by Rutherford backscattering (RBS). At $T_s=900$ °C, AlN nucleated in the (111)-oriented cubic 3C polytype which persisted for 6–8 layers (1.5–2 nm) prior to growth of the (0001)-oriented hexagonal 2H polytype. The epitaxial relationship was found by cross-sectional transmission electron microscopy (XTEM) and XRD to be 2H–AlN(0001)//3C–AlN(111)// Si(111) with 2H–AlN[$1\bar{2}10$]//3C–AlN[110]//Si[110].

II. EXPERIMENTAL PROCEDURE

All films were grown in a magnetron sputter deposition system with a base pressure of 2×10^{-7} Torr which has been described in detail elsewhere.[17] The target was a 99.95% pure Al disk, 150 mm in diameter by 10 mm thick, separated by 80 mm from the resistively heated graphite substrate holder. A rotatable shutter is positioned directly above the substrate in order to allow sputter cleaning of the target surface and plasma stabilization prior to initiating deposition. The system is equipped with an external Helmholz magnet, in addition to the permanent magnets in the magnetron, in order to operate in a controlled magnetically unbalanced mode.

The substrates were Si(111) wafers with a resistivity of 4–6 Ω cm. They were cleaned by first dipping them in a 10% HF aqueous solution, rinsing them in de-ionized water, and drying them in dry N_2. The wafers were then inserted into the deposition system and heated to 850 °C for 10 min in vacuum to remove the surface oxide prior to setting the desired growth temperature T_s. A dummy Si substrate on which a Chromel–Alumel thermocouple was clamped was used to monitor the growth temperature during deposition.

Ar (99.9999% pure) was introduced into the sputtering system to a pressure $P_{Ar}=1.50$ mTorr as determined by a capacitance manometer. N_2 was then added to obtain the desired gas composition. Typical operation conditions were: target current $I_T=1$ A; target voltage $V_T=295$ V; and nitrogen partial pressure $P_{N_2}=0.25$ mTorr. This set of conditions resulted in an AlN deposition rate of 2.1 μm h^{-1}.

The RBS measurements were performed in an UHV ion-beam analysis chamber which was equipped with electric and magnetic secondary electron suppression. The dose obtained by integrating the current was 5 μC and the measurement precision was better than 0.1%. The AlN sample compositions were determined by comparing the measured scattering yields to those obtained from a pure Al reference sample. The uncertainty in composition determination is governed by the accuracy of tabulated values for the specific energy loss for N.[18] Typically uncertainties in tabulated energy loss values are of the order of 5% yielding an accuracy in the present measurements of better than 2%. To reduce the uncertainty further, we measured the yield at different He^+ beam energies (2, 3, and 3.75 MeV). From these analyses measured N/Al ratios agreed within 0.01. Thus, we can conclude that the uncertainties in the α-particle energy loss due to N were overestimated and the measurement uncertainty is less than 1%.

As-deposited films were analyzed structurally by XRD and XTEM. The XRD analyses were initially carried out using Cu Kα radiation in a conventional powder diffractometer with a resolution of 0.01 °2Θ and independent Θ and 2Θ motion. High-resolution reciprocal space mapping, texture scans, and conventional rocking curve analyses were conducted using a Philips Materials Research (MRD) diffractometer equipped with a Eulerian cradle. In the high-resolution triple-axis mode employed for mapping, a four-crystal monochromator consisting of grooved Ge(220) crystals was utilized to provide a resolution of 0.001 °2Θ with Cu Kα_1 while the resolution was 0.01 °2Θ in the parallel-beam configuration.

XTEM analyses were conducted using a Philips CM 20 UT microscope operated at 200 kV. Sample preparation for XTEM consisted of gluing two specimens together film to film. The sample was then ground and polished to a thickness of about 60 μm. Final thinning was done from both sides using two 3 keV Ar^+-ion beams at a low incidence angle of 7° in order to minimize differential film/substrate etching rates.

The average roughnesses of as-deposited samples were determined by scanning force microscopy (SFM) using a Nanoscope system with microfabricated Si tip/cantilevers.

III. EXPERIMENTAL RESULTS AND DISCUSSION

A. Film growth

N_2 gas consumption ΔP_{N_2} and target voltages V_T during reactive sputter deposition of Al in mixed Ar+N_2 discharges are plotted in Fig. 1 as a function of residual N_2 partial pressure $\delta P_{N_2}=(P_{N_2}-\Delta P_{N_2})$. The Ar pressure and target current were maintained constant at 1.50 mTorr and 1 A, respectively. The behavior of ΔP_{N_2} vs δP_{N_2} is in agreement with

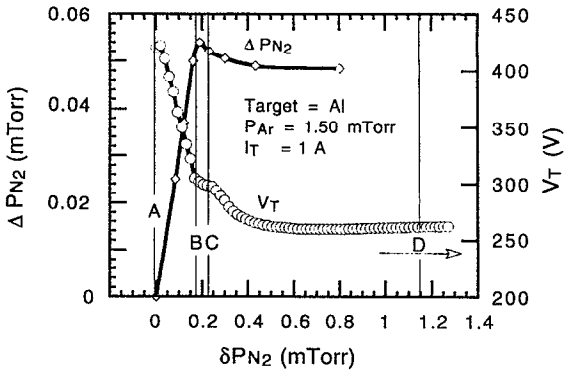

FIG. 1. Dependence of nitrogen gas "consumption" ΔP_{N_2} and target voltage V_T on the N_2 partial pressure difference $\delta P_{N_2}=(P_{N_2}-\Delta P_{N_2})$ during reactive sputter deposition from an Al target in mixed Ar+N_2 discharges at a constant Ar pressure of 1.5 mTorr.

predictions based upon general models of reactive sputtering[19,20] while the variation of $V_T(\delta P_{N_2})$ in constant current mode is shown below to be a relatively simple and effective indicator of the deposition conditions necessary for obtaining stoichiometric AlN layers from a partially nitrided target.

The plot of V_T vs δP_{N_2} in Fig. 1 can be divided into three regions separated by vertical lines labeled A, B, C, and D. In region A–B, ΔP_{N_2} increases approximately linearly from 0 in pure Ar discharges to 0.05 mTorr at $\delta P_{N_2}=0.18$ mTorr while V_T decreases linearly from 420 to 300 V. The latter is consistent with results in Ref. 16 showing that the secondary electron yield γ from Al targets increases with increasing nitrogen coverage. Since we are using a regulated constant current power supply, V_T decreases in response to increasing γ. In this regime, essentially all N_2 flowing into the deposition system is absorbed by deposited Al as the chamber walls and fixtures act as an internal sorption pump.

At point B, the input N_2 flow begins to exceed the pumping capability of the deposited Al and excess N_2 rapidly nitrides the remaining free Al on the target surface. Thus, the region B–C in Fig. 1 corresponds to the rather narrow N_2 partial pressure range over which the partially nitrided target surface (point B) is converted into a fully nitrided surface (point C). V_T continues to decrease in this regime, but at a less rapid rate than in region A–B. The N_2 consumption in B–C remains approximately constant, or decreases slightly, as the flux of sputtered Al atoms from the target decreases. This behavior is similar to results obtained for the reactive magnetron sputtering of Ti in mixed Ar+N_2 discharges.[20] Throughout the following regime C–D, in which the target remains fully nitrided (i.e., "poisoned"), changes in V_T with increasing δP_{N_2} are controlled primarily by competing plasma volume effects. That is, while V_T is expected to decrease with increasing total pressure, it increases slightly with increasing N_2 partial pressure due to the smaller electron impact ionization cross section of N_2 than of Ar.[21]

Figure 2 shows changes in V_T with $P_{Ar}=1.50$ mTorr and $\delta P_{N_2}=$(1) 0, (2) 0.13, (3) 0.16, (4) 0.18, and (5) 0.22 mTorr as I_T was varied at a constant rate of 1.2 A min^{-1}. The ar-

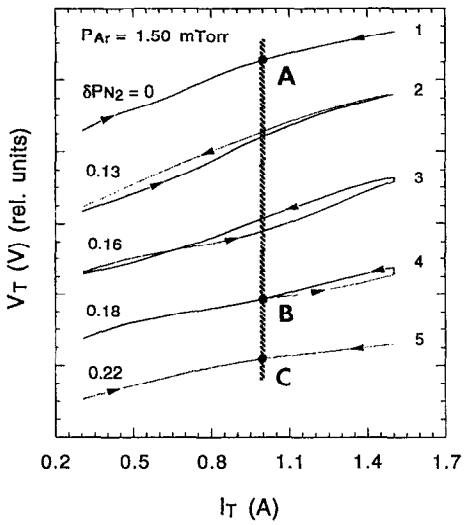

FIG. 2. Relative variation of the target voltage V_T vs target current I_T during reactive sputter deposition from an Al target in mixed $Ar+N_2$ discharges at δP_{N_2} values of (1) 0, (2) 0.13, (3) 0.16, (4) 0.18, and (5) 0.22 mTorr. The Argon partial pressure P_{Ar} was maintained constant at 1.5 mTorr and I_T was varied both positively and negatively at a constant rate of 1.2 A min^{-1}.

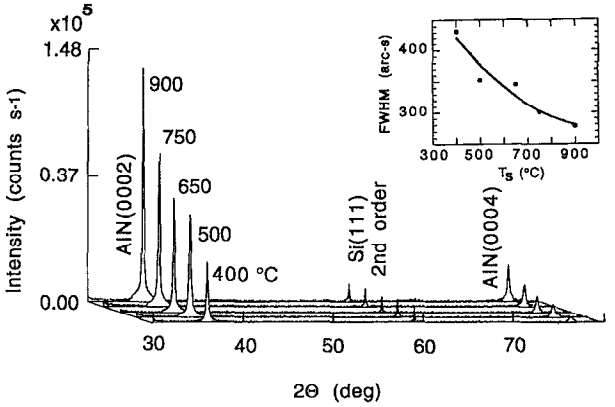

FIG. 3. Θ-2Θ XRD scans from AlN(0002) films grown on Si(111) at temperatures T_s ranging from 400 to 900 °C under plasma conditions corresponding to point B in Figs. 1 and 2.

rowheads indicate the direction of the change while the vertical line corresponds to a target current I_T=1 A and can be correlated with the $\Delta N_2 - \delta P_{N_2}$ and $V_T - \delta P_{N_2}$ curves in Fig. 1 through the points labeled A, B, and C. Similar S-shaped $V_T - I_T$ curves have been discussed by Steenbeck and co-workers[19] as a transition between two target states: a clean Al target, curve 1, and a fully nitrided target surface, curve 5. There is essentially no measurable hysteresis in curves 1 and 5 while intermediate curves exhibit the type of hysteretic behavior typically observed during reactive sputtering of gas–metal systems with large enthalpies of compound formation.[23]

Over the region A–B (Fig. 1), there is a systematic shift of the hysteresis loop (Fig. 2) toward larger target currents with increasing δP_{N_2}. For a given δP_{N_2} value, in this regime, the current required to cause a change from a metallic to a partially nitrided target depends upon the direction of the change in I_T since ΔP_{N_2} is a function of the target surface composition.

Films grown under plasma conditions corresponding to point B (δP_{N_2}=0.18 mTorr) in Fig. 2 were found by RBS to be stoichiometric with a N/Al ratio of 1 within the resolution of the measurement technique, 0.01. However, decreasing δP_{N_2} by a relatively small amount to 0.16 mTorr at the same target current, I_T=1 A, resulted in the growth of an understoichiometric film with composition $Al_{0.53}N_{0.47}$. In fact, operation under δP_{N_2} conditions <0.18 mTorr (P_{N_2}<0.23 mTorr) with $I_T \leq 1$ A, at all growth temperatures used in this study, always resulted in Al-rich films of poor crystalline quality as determined by RBS and XRD. Moreover, with δP_{N_2}>0.22 mTorr (P_{N_2}>0.27 mTorr), the discharge became unstable and the deposition rate decreased substantially due to the formation of an increasingly thick dielectric layer on the target. Thus, a narrow region of nitrogen partial pressures near point B was found to be optimal for growth of stoichiometric AlN films from partially nitrided Al targets allowing growth rates of ≥ 2 μm h^{-1}.

B. Microstructure of epitaxial AlN

Figure 3 shows XRD patterns from 1.3-μm-thick AlN films deposited on Si(111) at growth temperatures between 400 and 900 °C under plasma conditions corresponding to point B in Figs. 1 and 2. The only film diffraction peaks observed are 0002 and 0004 showing that all layers exhibit strong (0001) preferred orientation. AlN 0002 peak positions, film lattice constants c, peak intensities I_{0002}, and FWHM values are listed in Table I. Increasing T_S over the range from 400 to 900 °C resulted in an increase in I_{0002}, from ~6000 to 148 000 counts s^{-1}, and a decrease in the FWHM of the Θ–2Θ AlN 0002 peak from 432 to 278 arc sec. Both results indicate a continuous increase in the crystalline quality with increasing growth temperature.

The measured c values in Table I for films grown at $T_s \leq 650$ °C are larger than the bulk lattice parameter of 0.4982 nm while films grown at higher temperatures exhibit c values which are 0.2% smaller than the bulk. This was expected, however, since the AlN thermal-expansion coefficient is larger than that of Si,[24] leading to the establishment of in-plane tensile differential thermal contraction upon cooling from the growth temperature. Assuming a biaxial stress

TABLE I. XRD results listing the AlN 0002 2Θ XRD peak position, the lattice constant c in the growth direction, the 0002 peak intensity I_{0002}, and FWHM values for AlN(0001) films grown on Si(111) by reactive magnetron sputter deposition at temperatures T_s between 400 and 900 °C under plasma conditions corresponding to point B in Figs. 1 and 2.

T_s (°C)	0002 (°2Θ)	c (nm)	I_{0002} (count s^{-1})	FWHM (arc sec)
400	35.960	0.4991	6068	432
500	35.915	0.4997	24 586	352
650	35.915	0.4997	30 346	345
750	36.125	0.4969	60 565	301
900	36.100	0.4972	148 456	278

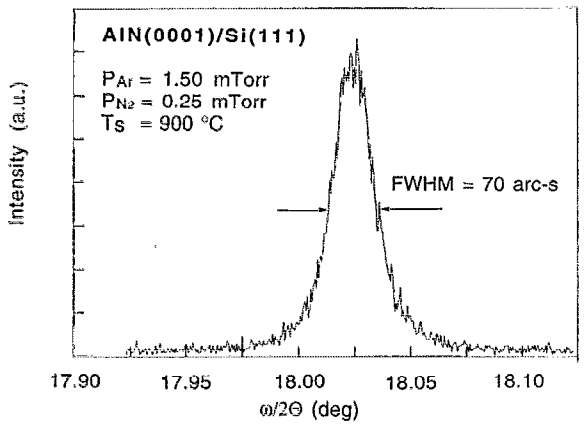

FIG. 4. A typical θ-2Θ rocking curve for an AlN(0002) film grown on Si(111) at T_s=900 °C.

state, a Poission ratio of 0.3, and no stress relaxation, the actual c values of T_s=750 and 900 °C films are identical to the bulk after accounting for the differential thermal stress. However, for films grown at $T_s \leq 650$ °C, subtraction of the thermal stress leads to c values, ranging from 0.4996 to 0.5003 nm, which are larger than that of the bulk indicating the presence of compressive growth stresses which are most likely due to small deviations from stoichiometry and/or the presence of residual defects.

A typical 0002 $\omega-2\Theta$ rocking curve obtained using the high-resolution diffractometer in the triple-axis configuration from an AlN film grown at T_s=900 °C is shown in Fig. 4. The FWHM value is 70 arcsec, only six times wider than that obtained for the Si 111 substrate peak, ~12 arc sec. The in-plane coherence length Δx of AlN(0002) basal planes was determined from the ω rocking curve FWHM to be 18–20 nm. A Φ scan from an asymmetric AlN 1013 peak is reproduced in Fig. 5. The pattern was obtained using the high-resolution diffractometer in the parallel-beam mode with ω and 2Θ angles optimized for the AlN 0002 peak. The sixfold symmetry of the wurtzite-structure crystal basal plane is clearly revealed by the six 60°-separated peaks.

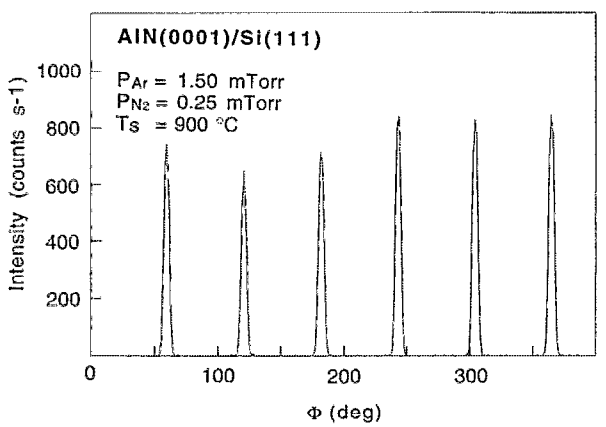

FIG. 5. A ϕ scan about the AlN 1013 diffraction peak from an AlN film grown on Si(111) at T_s=900 °C.

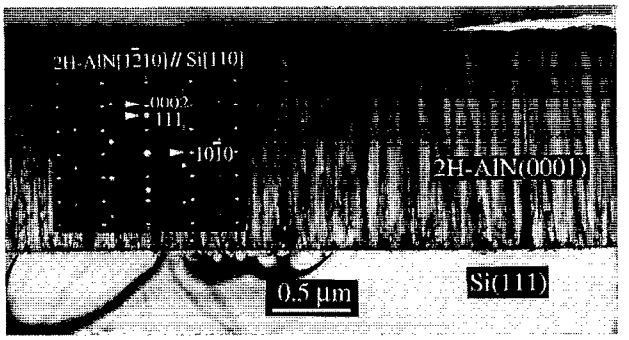

FIG. 6. A cross-sectional transmission electron micrograph with corresponding selected-area electron-diffraction pattern from an AlN(0001) film grown on Si(111) at T_s=900 °C.

Figure 6 is an XTEM micrograph with a corresponding selected-area electron-diffraction (SAED) pattern from the T_s=900 °C AlN film used to obtain the XRD results in Fig. 5. The position of the diffraction spots and the symmetry of the pattern are consistent with the XRD results above and give an orientational relationship between film and substrate of 2H–AlN(0001)//Si(111) with 2H–AlN[1$\bar{2}$10]//Si[110]. The columnar-type structure shown in the XTEM micrograph of Fig. 6 is due to a combination of double-positioning domains and low-angle grain boundaries extending in the growth direction. The columns, which have diameters of ~50 nm, are faceted at the top surface exhibiting a pyramidal shape with a root-mean-square surface roughness of ~10 nm as determined by SFM.

A typical double-positioning domain boundary (DPB) is shown in the high-resolution micrograph in Fig. 7. The DPB represents the difference in stacking sequence between 2H–AlN columns with stacking sequences ···ABAB··· and ···BABA··· . In the [1$\bar{2}$10] projection shown, the boundary is inclined. Tanaka, Kern and Davis[25] recently reported the formation of DPBs in a thin 2H–AlN film grown by plasma-assisted gas-source molecular-beam epitaxy on SiC(0001).

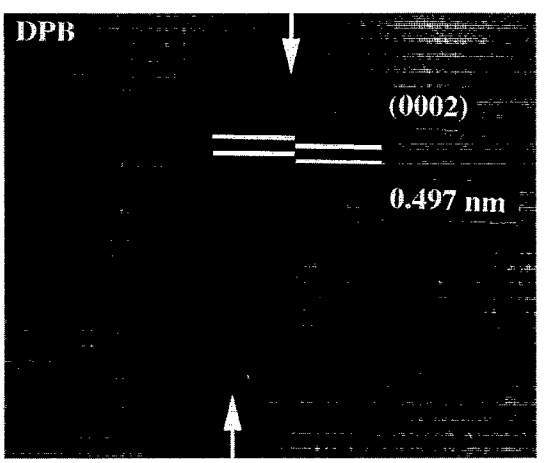

FIG. 7. A high-resolution cross-sectional transmission electron image of an AlN(0001) film showing a double-positioning domain boundary (DPB) (labeled with arrows). The difference in stacking sequence across the boundary is indicated by black and white bars.

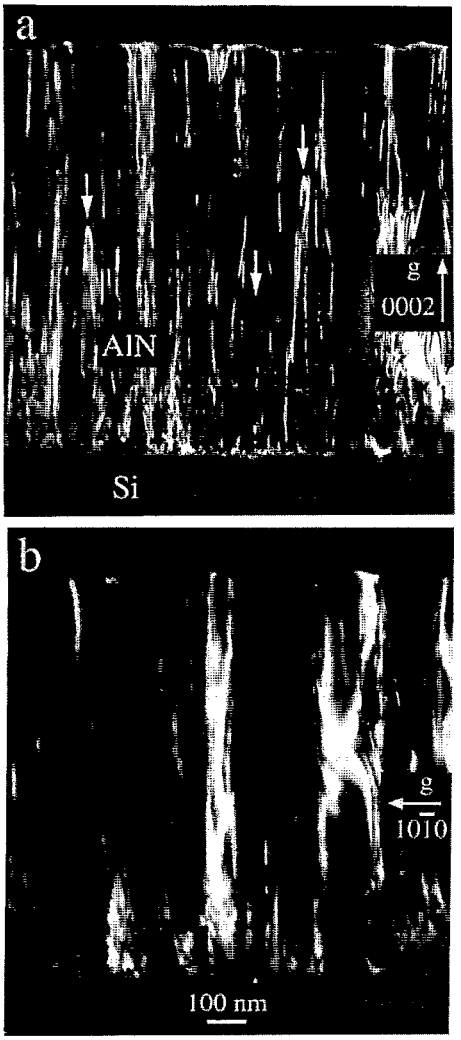

FIG. 8. $[1\bar{2}10]$ dark-field weak-beam images taken from the same region of an AlN(0002) film as that shown in Fig. 7. With diffraction vectors (a) $\mathbf{g}=[0002]$ and (b) $\mathbf{g}=[10\bar{1}0]$. Dislocations terminating within the film and giving rise to half-loops are marked by arrows in (a).

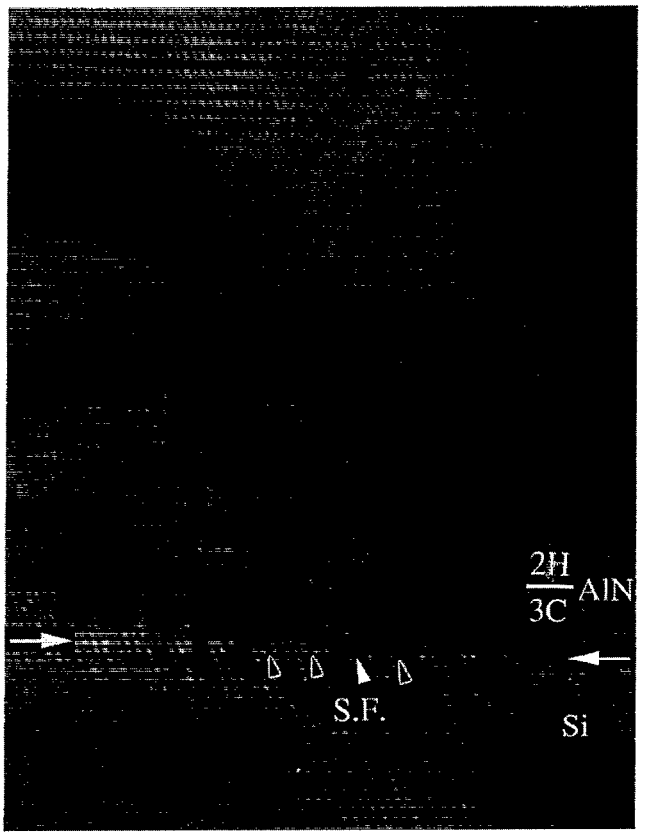

FIG. 9. A high-resolution cross-sectional transmission electron micrograph of an AlN(0001) film grown on Si(111) (interface indicated by arrows) at T_s=900 °C. The film was initially 3C cubic before transforming to the hexagonal 2H polytype after growth of 6–8 layers. Misfit dislocations and stacking faults at the 3C–AlN/Si interface are labeled by arrowheads and the symbol "S.F.", respectively.

The combination of the relaxation of atoms at DPBs and the mosaic structure from columns rotated around the surface normal gave rise to the in-plane elongation of the AlN diffraction spots in Fig. 6.

Figures 8(a) and 8(b) are $[1\bar{2}10]$ dark-field weak-beam images obtained with diffracting vectors (a) $\mathbf{g}=[0002]$ and (b) $\mathbf{g}=[10\bar{1}0]$. Figure 8(a) shows that the column domains are bounded by dislocations with curved dislocations lines which originate near the interface to the Si substrate and extend in the growth direction. Some dislocations [examples are marked by arrows in Fig. 8(a)] terminate within the film and give rise to half-loops. In Fig. 8(b), the dominant contrast is due to extended DPBs which have their displacement vectors in the film plane. However, some of the dislocations which exhibit very strong contrast in Fig. 8(a) are also visible in Fig. 8(b). Dark-field fault analyses using the $[1\bar{2}10]$ and $[0\bar{1}10]$ zone axes with $\mathbf{g}=[0002]$, $[10\bar{1}0]$, $[11\bar{2}0]$ and $[10\bar{1}1]$ did not result in complete extinction of any dislocations in Fig. 8 indicating that they have mixed edge and screw character. The dominant character was of screw type, however, since the strongest contrast was observed with $\mathbf{g}=[0002]$.

Figure 9 is a typical high-resolution XTEM image from the AlN/Si interface. In all resolvable areas, AlN was observed to nucleate and grow in the (111)-oriented cubic 3C polytype for 6–8 layers (1.5–2 nm) before transforming to the (0001)-oriented 2H polytype. The regularly spaced misfit dislocations at the 3C–AlN/Si interface, marked by arrowheads in Fig. 9, indicate that the films are at least partially relaxed (the AlN and Si lattice constant mismatch is 20%). Stacking faults (labeled "S.F." in Fig. 9) were also observed in the 3C–AlN layer.

No DPBs were detected in the 3C–AlN layer. Such defects at a close-packed interface such as 3C–AlN/Si(111) would have been observable in high-resolution XTEM images with the appearance of a twin boundary between domains having stacking sequences[26] ···ABCABC··· and ···BACBAC··· . Thus, we propose that the DPBs which we observe in the 2H–AlN epitaxial layers originate at the 3C–AlN/2H–AlN interface due to 2H growth on differently terminated steps ···A, B, and/or C··· on the 3C–AlN surface. The 3C–AlN step configuration was, in turn, determined during coalescence and relaxation of the initial 3C–domains.

IV. CONCLUSIONS

(1) Measurements of target voltage–current characteristics together with the measured nitrogen gas consumption during growth of AlN by reactive magnetron sputter deposition was used to reproducibly control deposition in order to obtain stoichiometric films.

(2) High structural quality epitaxial AlN(0001) films were grown on Si(111). XRD $\omega-2\Theta$ and ω rocking curve widths of 70 and 500 arc sec, the lowest values yet reported, were obtained from films grown at T_s=900 °C.

(3) The primary defects observed were double-positioning domain boundaries and low-angle grain boundaries bounded by dislocations with a mixed screw and edge character.

(4) AlN was found to nucleate in a metastable (111)-oriented cubic 3C polytype which persisted for 6–8 layers (1.5–2 nm) before transforming to the hexagonal (0001)-oriented 2H polytype.

(5) The overall AlN/Si epitaxial relationship was 2H–AlN(0001)//3C–AlN(111)//Si(111) with 2H–AlN[$1\bar{2}10$]// 3C–AlN[110]//Si[110].

ACKNOWLEDGMENTS

The authors gratefully acknowledge the financial support of the Swedish Natural Research Council (NFR), the Material Research Consortium on "Thin Film Growth" (financed jointly by the Swedish Board for Technical Development, NUTEK, and NFR), the U.S. Joint Services Electronics Program, and the U.S. Department of Energy. Mats Johansson and K. Brolin are acknowledged for their help with TEM sample preparation and for technical assistance, respectively.

[1] I. Petrov, E. Mojab, R. C. Powel, J.-E. Greene, L. Hultman, and J.-E. Sundgren, Appl. Phys. Lett. **60**, 2491 (1992).
[2] S. Kaneko, M. Tanaka, K. Masu, K. Tsubouchi, and N. Mikoshiba, J. Cryst. Growth **115**, 643 (1991).
[3] W. Yim, E. Stofko, P. Zanzucchi, J. Pankov, M. Ettenberg, and S. Gillbert, J. Appl. Phys. **44**, 292 (1973).
[4] S. Yoshida, S. Misawa, Y. Fudjii, S. Takada, H. Hayakawa, S. Gonda, and A. Itoh, J. Vac. Sci. Technol. **16**, 990 (1979).
[5] G. Nyberg and R. Burhman, J. Vac. Sci. Technol. A **2**, 301 (1984).
[6] H. T. G. Hentzell, J. M. E. Harper, and J. J. Cuomo, J. Appl. Phys. **58**, 556 (1985).
[7] T. Shiosaki, T. Yamamoto, T. Oda, and A. Kawabata, Appl. Phys. Lett. **36**, 643 (1980).
[8] X. Wang, K. Hipps, and U. Mazur, Langmuir **8**, 1347 (1992).
[9] E. Rille, Z. Zarwasch, and H. K. Pulker, Thin Solid Films **228**, 215 (1993).
[10] W. J. Meng, J. Heremans, and Y. T. Cheng, Appl. Phys. Lett. **59**, 2097 (1991).
[11] A. Saxler, P. Kung, C. J. Sun, E. Bigan, and M. Razegi, Appl. Phys. Lett. **64**, 339 (1994).
[12] W. J. Meng, J. A. Sell, and R. A. Waldo, J. Vac. Sci. Technol. A **9**, 2183 (1991).
[13] G. L. Huffman, D. E. Fahnline, R. Messier, and L. J. Pilione, J. Vac. Sci. Technol. A **7**, 2252 (1989).
[14] T. Takahashi, F. Takeda, and M. Naoe, Mater. Res. Soc. Symp. Proc. **167**, 277 (1990).
[15] F. C. Stedile, I. J. R. Boumvol, W. H. Schreiner, and F. L. Freire, Jr., Nucl. Instrum. Methods B **79**, 501 (1993).
[16] M. Lewis, D. Glocker, and J. Jorne, J. Vac. Sci. Technol. A **7**, 1019 (1989).
[17] I. Ivanov, P. Kazansky, L. Hultman, I. Petrov, and J.-E. Sundgren, J. Vac. Sci. Technol. A **12**, 315 (1994).
[18] J. F. Ziegler, J. P. Biersack, and U. Littmark, *The Stopping Range of Ions in Solids* (Pergamon, New York, 1985), Vol. 1.
[19] K. Steenbeck, E. Steibeiss, and K.-D. Ufert, Thin Solid Films **92**, 371 (1982).
[20] S. Berg, T. Larsson, C. Nender, and H.-O. Blom, J. Appl. Phys. **63**, 887 (1988).
[21] I. Petrov, A. Myers, J. E. Greene, and J. R. Abelson, J. Vac. Sci. Technol. A **12**, 2846 (1994).
[22] D. Rapp and P. Englander-Golden, J. Chem. Phys. **43**, 1464 (1965).
[23] A. H. Eltoukhy, B. R. Natarjan, J. E. Greene, and T. L. Barr, Thin Solid Films **69**, 229 (1980).
[24] S. Strite and H. Morkoç, J. Vac. Sci. Technol. B **10**, 1237 (1992).
[25] S. Tanaka, R. S. Kern, and R. F. Davis, Appl. Phys. Lett. **66**, 37 (1995).
[26] Q. Wahab, L. Hultman, I. P. Ivanov, M. Willander, and J.-E. Sundgren, Thin Solid Films (to be published).